Article:

Lunt, DJ, Haywood, AM, Schmidt, GA et al. (3 more authors) (2012) On the causes of mid-Pliocene warmth and polar amplification. Earth and Planetary Science Letters, 321-32 (8). 128 - 138. ISSN 0012-821X

https://doi.org/10.1016/j.epsl.2011.12.042

On the causes of mid-Pliocene warmth and polar amplification

Daniel J. Lunt[(1,*)], Alan M. Haywood[(2)], Gavin A. Schmidt[(3)], Ulrich Salzmann[(4)], Paul J. Valdes[(1)], Harry J. Dowsett[(5)], Claire A. Loptson[(1)]

(1) School of Geographical Sciences
University of Bristol
University Road
Bristol BS8 1SS, UK

(2) School of Earth and Environment
Woodhouse Lane
University of Leeds
Leeds LS2 9JT, UK

(3) NASA/Goddard Institute for Space Studies
2880 Broadway
New York
NY 10025, USA

(4) School of the Built and Natural Environment
Northumbria University
Newcastle upon Tyne NE1 8ST, UK

(5) U.S. Geological Survey
12201 Sunrise Valley Drive MS926A
Reston
VA 20192, USA

(*) Corresponding author:
Email: d.j.lunt@bristol.ac.uk
Tel: +44 (0) 117 3317483
Fax: +44 (0) 117 9287878

1 Abstract

The mid-Pliocene (∼ 3 to 3.3 million years ago), is a period of sustained global warmth in comparison to the late Quaternary (0 to ∼ 1 million years ago), and has potential to inform predictions of long-term future climate change. However, given that several processes potentially contributed, relatively little is understood about the reasons for the observed warmth, or the associated polar amplification. Here, using a modelling approach and a novel factorisation method, we assess the relative contributions to mid-Pliocene warmth from: elevated CO_2, lowered orography, and vegetation and ice sheet changes. The results show that on a global scale, the largest contributer to mid-Pliocene warmth is elevated CO_2. However, in terms of polar amplification, changes to ice sheets contribute significantly in the Southern Hemisphere, and orographic changes contribute significantly in the Northern Hemisphere. We also carry out an energy balance analysis which indicates that that on a global scale, surface albedo and atmospheric emmissivity changes dominate over cloud changes. We investigate the sensitivity of our results to uncertainties in the prescribed CO_2 and orographic changes, to derive uncertainty ranges for the various contributing processes.

2 Introduction

The most recent palaeoclimate reconstructions (Dowsett *et al.*, 2009) suggest that during warm 'interglacials' of the Pliocene epoch (∼5.3 to 2.6 Ma), global annual mean sea surface temperatures were 2 to 3 °C higher than the pre-industrial era. During these warm interglacials sea levels were higher than today (estimated to be 10 to 30+ metres) meaning that global ice volume was reduced (e.g. Dowsett and Cronin, 1990; Naish and Wilson, 2009; Dwyer and Chandler, 2009). There were large fluctuations in ice cover on Greenland and West Antarctica, and during the interglacials they were probably largely free of ice (Lunt *et al.*, 2008; Pollard and DeConto, 2009; Hill *et al.*, 2010;

Dolan *et al.*, 2011). Some ice may also have been lost from around the margins of East Antarctica especially in the Aurora and Wilkes sub-glacial basins (Hill *et al.*, 2007). Coniferous forests replaced tundra in the high latitudes of the Northern Hemisphere (Salzmann *et al.*, 2008), and the Arctic Ocean may have been seasonally free of sea-ice (e.g. Cronin *et al.*, 1993). The most recent estimates of Pliocene atmospheric CO_2 concentrations range between 280 and 450 ppmv (Pagani *et al.*, 2010; Seki *et al.*, 2010). The Mid-Piacenzian Warm Period (henceforth 'mid-Pliocene'; 3.26 to 3.025 Ma BP; timescale of Lisiecki and Raymo (2005)) is a particularly well documented interval of warmth during the Pliocene, with global data sets of multi-proxy sea surface temperatures, bottom water temperatures, vegetation cover, topography and ice volume readily available as boundary conditions and/or evaluation datasets for global climate models (Dowsett *et al.*, 2010b; Haywood *et al.*, 2010).

Many parallels have been drawn between the apparent similarities in climate between warm intervals of the Pliocene and the end of the 21st Century, particularly in terms of (relative to pre-industrial) (a) the change in annual mean global temperature (Jansen *et al.*, 2007; Haywood *et al.*, 2000a), (b) changing meridional surface temperature profiles showing a strong polar amplification of the warming (Dowsett *et al.*, 1992; Robinson, 2009), (c) changing precipitation patterns and storm tracks (Haywood *et al.*, 2000b) and even (d) Hurricane intensity and ENSO-event frequency/extra tropical teleconnections (Fedorov *et al.*, 2010; Bonham *et al.*, 2009; Scroxton *et al.*, 2011; Watanabe *et al.*, 2011). This attraction is made more intense by the fact the continents had essentially reached their modern position, and due to its relative youth, geologically speaking, inferences about the environmental tolerances of many of the biological proxies used to reconstruct Pliocene environments and climates can be made with far greater confidence than further back in Earth history (Dowsett and Poore, 1996; Salzmann *et al.*, 2008).

As such, it is particularly important to understand *why* the mid-Pliocene was warmer than pre-industrial. Up until now, the most comprehensive attempt to answer this question was carried out by Haywood and Valdes (2004), henceforth H&V04. Using the UK Met Office coupled atmosphere-ocean General Circulation model, HadCM3, they carried out a model simulation of the mid-Pliocene, and compared it to a pre-industrial simulation. They found a global mean surface air temperature difference of 3.1°C. From the assumed CO_2 radiative forcing in the model and consideration of top-of-the-atmosphere radiative fluxes, they partitioned the causes of this temperature difference between CO_2 (1.9 Wm^{-2}), surface albedo (2.3 Wm^{-2}) and cloud cover (1.8 Wm^{-2}) changes. They further partitioned the surface albedo component between land ice and snow (55%) and sea ice (45%) changes. From interrogating the ocean streamfunction and net heat transports, they also concluded that ocean circulation changes did not lead to significant surface temperature warming. Given the considerable computational constraints at the time (the 300 year simulation took 9 months to complete), the H&V04 study contributed significantly to our understanding of the causes of mid-Pliocene warmth. However, the fact that further sensitivity studies could not be carried out meant that cause and effect was not easily partitioned. For example, the albedo change due to sea ice was itself a result of the imposed CO_2 (and orography, and vegetation, and land-ice) changes. Similarly for clouds - some of the cloud changes would be due to the land ice (and other) changes. In this paper we address this issue, by describing a new methodology for a robust, self-consistent partitioning of climate change between several causal factors. We then apply it to the warm periods of the mid-Pliocene, resulting in a partitioning of temperature changes between changes in the prescribed CO_2, orography, vegetation and ice sheet boundary conditions. We also carry out an analysis of the pre-industrial and mid-Pliocene results using an energy balance method described by Heinemann *et al.* (2009).

3 Experimental Design

3.1 Model Description - HadCM3

All the General Circulation Model (GCM) simulations described in this paper are carried out using the UK Met Office coupled ocean-atmosphere GCM HadCM3, version 4.5 (Gordon *et al.*, 2000). The resolution of the atmospheric and land components is 3.75° in longitude by 2.5° in latitude, with 19 vertical levels in the atmosphere. The resolution of the ocean model is 1.25° by 1.25° with 20 levels in the vertical. Parameterisations include the radiation scheme of Edwards and Slingo (1996), the convection scheme of Gregory *et al.* (1997), and the MOSES-1 land-surface scheme, whose representation of evaporation includes the dependence of stomatal resistance on temperature, vapour pressure and CO_2 concentration (Cox *et al.*, 1999). The ocean model uses the Gent and McWilliams (1990) mixing scheme. There is no explicit horizontal tracer diffusion in the model. The horizontal resolution allows the use of a smaller coefficient of horizontal momentum viscosity leading to an improved simulation of ocean velocities compared to earlier versions of the model. The sea ice model uses a simple thermodynamic scheme and contains parameterisations of ice concentration (Hibler, 1979) and ice drift and leads (Cattle and Crossley, 1995). In simulations of the present-day climate, the model has been shown to simulate SST in good agreement with modern observations, without the need for flux corrections (Gregory and Mitchell, 1997). Future climate predictions from the model were presented in the latest IPCC report (Solomon *et al.*, 2007), and it has been used in the Palaeoclimate Modelling Intercomparison Project to simulate Last Glacial Maximum and Mid-Holocene climates (Braconnot *et al.*, 2007). The model will also be used in the forthcoming PlioMIP project (Haywood *et al.*, 2010, 2011b).

3.2 Boundary Conditions

The PRISM project (http://geology.er.usgs.gov/eespteam/prism/) has as its main aim the characterisation of the palaeoenvironment of the mid-Pliocene warm period (3.26 - 3.025 Ma) on a global scale. In this paper, we simulate the mid-Pliocene climate by making use of the PRISM2 reconstruction of orography, vegetation, and ice sheet extent (Dowsett *et al.*, 1999; Dowsett, 2007), which are described below.

The PRISM2 orography reconstruction was based on palaeobotanical evidence suggesting that the

East African rift areas were 500 m higher during the mid-Pliocene relative to today (Thompson and Fleming, 1996). In contrast, palaeoelevation of the Western Cordillera of North America and northern South America was reduced by 50%. Large elevation differences are noted in both Greenland and Antarctica due to significant removal of continental ice (Dowsett *et al.*, 1994; Dowsett, 2007). PRISM2 land ice distribution and volume was closely associated with sea level estimates from several sources (see Dowsett, 2007), which indicate a eustatic sea level rise of around 25 m compared to modern. These estimates have recently been confirmed by independent studies based on the depth palaeoecology of foram assemblages from New Zealand (Naish and Wilson, 2009) and benthic Mg/Ca and oxygen isotopes (Dwyer and Chandler, 2009). Antarctic ice distribution was based upon a modelled stable ice sheet configuration (see Dowsett *et al.*, 1999), strongly constrained by the sea-level reconstructions. The PRISM2 vegetation reconstruction (Dowsett *et al.*, 1999) was compiled from fossil pollen and plant macrofossil data from 74 sites covering all continents. PRISM2 vegetation is identical to PRISM1 (see Thompson and Fleming, 1996). PRISM2 uses seven land cover categories (desert, tundra, grassland, deciduous forest, coniferous forest, rainforest, and land ice) that are a simplification of the 22 land cover types of Matthews (1985). From the PRISM2 vegetation, orography, and ice-sheet extent, we derive all the boundary conditions necessary to run the GCM in mid-Pliocene mode (a total of 23 variables different to those of the pre-industrial, such as heat capacity of the soil, albedo, moisture holding capacity etc.).

Since the development of the PRISM2 dataset, the USGS have now released an updated version - PRISM3 (Dowsett *et al.*, 2010b,a). We use the PRISM2 dataset; firstly, to maintain consistency with previous modelling studies, in particular H&V04 and Lunt *et al.* (2010a); secondly, the mid-Pliocene simulation with PRISM2 boundary conditions has been spun up for a total of over 1000 years, which is considerably more than could be achieved with new boundary conditions in a reasonable timeframe. In section 5.1 we discuss the implications for this study of using PRISM2 compared to PRISM3 boundary conditions.

3.3 Factorisation Methodology

The primary aim of this study is to assess the relative importance of various boundary condition changes which contribute to mid-Pliocene warmth. Therefore, we are aiming to partition the total mid-Pliocene warming, ΔT, into four components, each due to the change in one of the boundary conditions CO_2, orography, ice sheet, and vegetation. The assumption here is that other palaeogeographic changes not currently captured by the PRISM dataset, such as soils or lakes, have a negligible impact on the global mean temperature change.

$$\Delta T = dT_{CO_2} + dT_{orog} + dT_{ice} + dT_{veg} \tag{1}$$

'Factor separation' techniques (e.g. Stein and Alpert, 1993) can be used to determine these components of the mid-Pliocene surface air temperature change dT_{CO_2}, dT_{orog}, dT_{veg}, and dT_{ice}. Typically, this involves carrying out an ensemble of GCM simulations with various combinations of boundary conditions. Here we present a new factorisation methodology, which we believe improves on previous work.

We name a GCM simulation which has boundary conditions x and y modified from pre-industrial to mid-Pliocene as E_{xy}. The four boundary conditions considered are atmospheric CO_2 (c), orography (o), vegetation (v), and ice sheets (i). Thus, a pre-industrial simulation is E, a mid-Pliocene simulation is E_{ociv}, and *e.g.* a simulation with pre-industrial ice sheets and vegetation but mid-Pliocene orography and CO_2 is E_{oc}. The corresponding surface air temperature distributions in these simulations we name T, T_{ociv}, and T_{oc} respectively.

For simplicity, we first describe our factorisation methodology by considering a simpler example, where only two boundary conditions (CO_2 and orography) are changed instead of four. The simplest factor separation technique is the incremental application of the boundary conditions. For our simplified example, this could involve an ensemble of 3 GCM simulations: E, E_c, and E_{oc}. The total temperature anomaly, ΔT (equal to T_{oc} - T in this simplified example), could be separated into 2 components:

$$\begin{aligned} dT_{CO_2} &= T_c - T \\ dT_{orog} &= T_{oc} - T_c, \end{aligned} \tag{2}$$

This method, illustrated in Figure 1a, has been used extensively in the climate literature (e.g., for the LGM see Broccoli and Manabe, 1987; von Deimling *et al.*, 2006). It has the advantage that a limited number of simulations ($N+1$, where N is the number of processes investigated) need be carried out. It has the disadvantage that it results in a non-unique solution: one could equally define

$$\begin{aligned} dT_{CO_2} &= T_{oc} - T_o \\ dT_{orog} &= T_o - T, \end{aligned} \tag{3}$$

which, due to non-linearities would in general result in a different partitioning.

Stein and Alpert (1993) (henceforth S&A93) recognised this and instead suggested that, considering the temperature response as a continuous function of two variables (in our simplified example orography and CO_2), and carrying out a Taylor expansion about the control climate, one can write

$$\Delta T = \frac{\partial T}{\partial CO_2}\Delta CO_2 + \frac{\partial T}{\partial orog}\Delta orog + nonlinear\ terms \tag{4}$$

They suggested that the nonlinear terms could be considered as 'synergy', S, between the two forcing variables, and that the partial derivatives be estimated from the GCM simulations relative to the control, so that

$$dT_{CO_2} = T_c - T$$

$$dT_{orog} = T_o - T$$
$$S = T_{oc} - T_o - T_c + T \tag{5}$$

This method, illustrated in Figure 1b, has been used in several previous studies (e.g. for the mid-Holocene and LGM see Wohlfahrt *et al.*, 2004; Jahn *et al.*, 2005). It has the advantage that it takes into account the non-linear interactions between the different boundary conditions. However, it requires a larger number of simulations (2^N) than the linear approach. Perhaps more importantly, it has the problem that it is not symmetric: one could equally carry out the Taylor expansion about the perturbed climate, and write

$$-dT_{CO_2} = T_o - T_{oc}$$
$$-dT_{orog} = T_c - T_{oc}$$
$$-S = T - T_o - T_c + T_{oc} \tag{6}$$

i.e. it would in general give a different answer if one asked “why is the mid-Pliocene warmer than pre-industrial” than if one asked “why is the pre-industrial cooler than the mid-Pliocene” (although the synergy term, S, would have the same magnitude in both cases).

In order to obtain a symmetric and unique factorisation, we instead estimate the partial derivatives in equation 4 with their average values over the domain considered, and write for our simplified case:

$$\begin{aligned} dT_{CO_2} &= \frac{1}{2}((T_c - T) + (T_{oc} - T_o)) \\ dT_{orog} &= \frac{1}{2}((T_o - T) + (T_{oc} - T_c)). \end{aligned} \tag{7}$$

This is equivalent to averaging the two different formulations of the S&A93 approach in Equations 5 and 6. An alternative, but identical, interpretation is that our technique uses the S&A93 formulation of Equation 5 but attributes the synergy term, S, equally between the two forcings:

$$\begin{aligned} dT_{CO_2} &= T_c - T + S/2 \\ dT_{orog} &= T_o - T + S/2 \\ (S &= T_{oc} - T_o - T_c + T) \end{aligned} \tag{8}$$

It is also equivalent to averaging the two linear formulations in Equations 2 and 3.

Our formulation has the advantage that it takes into account non-linear interactions, and is symmetric. In common with the S&A93 approach, it requires 2^N GCM simulations, and so is more computationally demanding than the linear approach.

For our mid-Pliocene study, where we actually have 4 variables (CO_2, orography, vegetation, and ice sheets), this would require 2^4=16 simulations. The factorisation would be as follows:

$$\begin{aligned} dT_{CO_2} = {} & \frac{1}{8}((T_c - T) + (T_{oc} - T_o) + (T_{ic} - T_i) + (T_{vc} - T_v) + \\ & (T_{ocv} - T_{ov}) + (T_{oci} - T_{oi}) + (T_{civ} - T_{iv}) + (T_{ociv} - T_{oiv})), \end{aligned} \tag{9}$$

$$\begin{aligned} dT_{orog} = {} & \frac{1}{8}((T_o - T) + (T_{co} - T_c) + (T_{io} - T_i) + (T_{vo} - T_v) + \\ & (T_{cov} - T_{cv}) + (T_{coi} - T_{ci}) + (T_{oiv} - T_{iv}) + (T_{coiv} - T_{civ})), \end{aligned} \tag{10}$$

$$\begin{aligned} dT_{veg} = {} & \frac{1}{8}((T_v - T) + (T_{cv} - T_c) + (T_{iv} - T_i) + (T_{ov} - T_o) + \\ & (T_{cvo} - T_{co}) + (T_{cvi} - T_{ci}) + (T_{vio} - T_{io}) + (T_{cvio} - T_{cio})), \end{aligned} \tag{11}$$

$$\begin{aligned} dT_{ice} = {} & \frac{1}{8}((T_i - T) + (T_{ci} - T_c) + (T_{vi} - T_v) + (T_{oi} - T_o) + \\ & (T_{cio} - T_{co}) + (T_{civ} - T_{cv}) + (T_{ivo} - T_{vo}) + (T_{civo} - T_{cvo})). \end{aligned} \tag{12}$$

Given the computational expense of carrying out 16 fully-coupled GCM simulations, we choose instead to consider CO_2/orography, and vegetation/ice sheets separately, and carry out two $N = 2$

factor separations (as in Equation 13), requiring only 7 simulations (illustrated in Figure 2).

$$
\begin{aligned}
dT_{CO_2} &= \frac{1}{2}((T_c - T) + (T_{oc} - T_o)), \\
dT_{orog} &= \frac{1}{2}((T_o - T) + (T_{oc} - T_c)), \\
dT_{veg} &= \frac{1}{2}((T_{ocv} - T_{oc}) + (T_{ociv} - T_{oci})), \\
dT_{ice} &= \frac{1}{2}((T_{oci} - T_{oc}) + (T_{ociv} - T_{ocv})).
\end{aligned} \tag{13}
$$

This factorisation is more computationally efficient than the full factorisation in Equation 12, but is not fully symmetric.

Five of these simulations (E, E_o, E_c, E_{oc}, E_{ociv}) were used in the study of Lunt *et al.* (2010a) in the context of deriving estimates of Earth system sensitivity, and the orography and snow-free surface albedo of these simulations are shown in their Table 1 of their Supplementary Information. The orography and snow-free albedo (an indicator of the land ice and vegetation distributions) for the 2 new simulations (E_{oci}, E_{ocv}), along with those for E and E_{ociv} for comparison, are shown in Figure 3. It is worth noting that because the ice sheets and vegetation are mutually exclusive in any one model grid cell, it is not possible to uniquely define boundary conditions for simulations E_{oci} and E_{ocv}. For the simulation with modern vegetation but Pliocene ice sheets (E_{oci}), in the regions which are ice sheet-free in the Pliocene but have ice sheets in the modern (e.g. the West Antarctic peninsula), it is not clear what albedo should be prescribed as there is no modern vegetation defined in these regions. Similarly, for the simulation with modern ice but Pliocene vegetation (E_{ocv}), in the same regions it is unclear whether to use the albedo of the Pliocene vegetation or of the modern ice. In other words, it is not well defined whether the albedo-induced warming associated with reduced ice sheets during the Pliocene is due to the reduction of ice *per se*, or due to the vegetation which replaces it. Here, we make the decision to attribute this warming to the vegetation that replaces it. As such, both simulations E_{oci} and E_{ocv} have the albedo of ice in regions which are ice-free in the Pliocene but have ice in the modern (Figure 3).

3.4 Mid-Pliocene model-data comparison

Before presenting and discussing our results, it is first important to have some confidence that the mid-Pliocene simulation, E_{ociv}, is consistent with observations of that period.

The SSTs in our mid-Pliocene simulation were evaluated relative to reconstructions of mid-Pliocene SST in Lunt *et al.* (2010a). They showed that the global mean SST change, mid-Pliocene minus pre-industrial, was well simulated (1.83°C in the model and 1.67°C in the observations). However, they also found that the latitudinal distribution of temperature change was not well simulated (their Figure 3c); the modelled mid-Pliocene warming being too great in the tropics and too small towards the poles. These discrepancies were investigated and discussed further in Dowsett *et al.* (2011).

A model-data comparison for the terrestrial climate, using a database of Pliocene palaeobotanical data (Salzmann *et al.*, 2008, 2009) was presented in the Supplementary Information of Lunt *et al.* (2010a). They found a fair agreement between E_{ociv} and the data on a global scale, with significantly improved skill at high latitudes in the E_{ociv} simulation compared with the pre-industrial E simulation.

4 Results

The temperature changes due to the CO_2 (dT_{CO_2}), orography (dT_{orog}), vegetation (dT_{veg}) and ice sheet (dT_{ice}) boundary condition changes, as calculated from equations 13, as well as the total change, ΔT, are illustrated in Figure 4. As a global average, of the total mid-Pliocene 3.3°C temperature change, 1.6°C (48%) is from the CO_2 (dT_{CO_2}), 0.7°C (21%) is from the orography (dT_{orog}), 0.7°C (21%) is from the vegetation (dT_{veg}), and 0.3°C (10%) is from the ice sheets (dT_{ice}).

dT_{CO_2} (Figure 4b) represents the temperature change due to CO_2 alone. It shares much in common with similar (CO_2 doubling as opposed to 280-400 ppmv here) results presented in the most recent report of the IPCC (Solomon *et al.*, 2007). For example, there is polar amplification due to snow and sea ice feedbacks, and greater temperature change on land compared to ocean due to reduced latent cooling and lower heat capacity. The North Atlantic shows reduced temperature increase due to ocean mixing and reduced northward heat transport in the Atlantic due to an increase in the intensity of the hydrological cycle. The increase of 1.6°C implies a climate sensitivity due to a doubling of CO_2 of ~3.2°C, which is close to the middle of the IPCC range (Solomon *et al.*, 2007). dT_{orog} (Figure 4c) highlights the local lapse-rate warming effect of the lower mid-Pliocene Rocky Mountain range. There is also a cooling to the west of the mid-Pliocene Canadian Rockies, associated with reduced precipitation and cloud cover, due to reduced ascent over the mountain range. There is a significant non-local effect of the lower Rockies - there is a large Arctic warming, in particular in the Barents Sea, which is amplified by reduced sea ice cover. This is due to a modification of the Rossby wave pattern, which is more zonally symmetric with the lower Rockies, indicated by a reduced trough over Greenland in the 500 mbar geopotential height field, consistent with previous work (e.g. Kutzbach *et al.*, 1989; Foster *et al.*, 2010). Very localised cooling associated with topographic effects are seen in the Andes, Himalayas, and East African rift valley regions. The surface ocean warming east of Japan is consistent with previous work showing this to be a region sensitive to orographic change in this model (Lunt *et al.*, 2010b). dT_{veg} (Figure 4c) shows that the largest vegetation-related temperature changes are in the Canadian Arctic, in particular Greenland (change from ice sheet to boreal forest), the Canadian archipelago (change from bare soil and glaciers to boreal forest), and Siberia (change from bare soil to boreal forest). This warming can be attributed to the relatively low albedo of boreal forest in the model, even when there is snow-cover on the ground. There are also large changes in the tropics, in particular in the Arabian peninsula, where the PRISM2 reconstruction indicates a shift from desert to grassland vegetation (based on pollen data (Van Campo, 1991)), resulting in a lower albedo in the mid-Pliocene than in the modern (see Figure 3). Some of the temperature changes attributed to vegetation will also be due to modifications to the roughness length, potential evapotranspiration, and other vegetation-spefcific model parameters. dT_{ice} (Figure 4d) shows warming in Greenland and parts of Antarctica due to a combination of lapse-rate, due to a lower mid-Pliocene ice sheet height, and albedo, due to the less reflective mid-Pliocene surface. The regions of Antarctic cooling are due to the fact that the PRISM ice sheet is higher in the Pliocene than in the modern in these regions. This is consistent with increased precipitation in the interior of the East Antarctic ice sheet in the warmer climate, and with modelled predictions for the future evolution of the Antarctic ice sheet under greenhouse gas forcing (e.g. Huybrechts *et al.*, 2004). The cooling in the Barents Sea is also consistent with previous work investigating the climatic effects of the removal of the Greenland ice sheet (Toniazzo *et al.*, 2004; Lunt *et al.*, 2004). However, apart from in this region, the signal due to the removal of the ice is very localised.

The results also allow us to ascertain the contribution to polar amplification of the four factors. We define polar amplification in this case to be any warming in the polar regions which is greater than the global mean warming. Figure 5(a) shows the same results as in Figure 4, but as zonal means. It is clear that the polar amplification in the Southern Hemisphere is due primarily to the ice sheet changes, whereas in the Northern Hemisphere it is due primarily to a combination of CO_2 and orography changes, with some contribution from vegetation around 60-70°N. Figures 1-3 in Supplementary Information illustrate the seasonality of the factorisation and polar amplification. It is clear that in the Northern Hemisphere, the polar amplification is dominated by an autumn and winter signal; in JJA there is almost no Northern Hemisphere polar amplification. In the Southern Hemipshere the seasonality is much more muted. These features are consistent with sea-ice and snow being the main causes of the seasonality.

It is interesting to assess the linearity of the climate system to these changes in boundary conditions. For example, to what extent does the temperature response of the system to a CO_2 change depend on the climate base state. Or, in other terms, how large is the 'synergy' term (S in Equation 5) in the S&A93 formulation? Figure 6 shows the two terms ($T_c - T$ and $T_{oc} - T_o$) which make up dT_{CO_2} in Equation 8, and the difference between them (S). The non-linearity is small compared to the temperature change itself, showing that in this case, the temperature response to an increase in CO_2 is largely independent of the orographic configuration. Similarly, the vegetation and ice sheet changes exhibit relatively small non-linearity (not shown). This implies that in this case, similar results could be obtained with a simple linear factorisation. However, it is not possible to know this *a priori*. The subtle non-linearities of the response of the system to changes in CO_2 alone are discussed in more detail in Haywood *et al.* (2011a).

It is also instructive to compare our results with those of H&V04. Our mid-Pliocene simulation differs from that of H&V04 for two reasons. Firstly, our simulation is a continuation of that of H&V04, and so is further spun-up and closer to equilibrium. Secondly, our simulation has been carried out over a number of 'real-world' years, and over this time has been migrated across several computers and Fortran compilers. Both hardware and compiler changes can affect the mean equilibrium climate of a model, due at least in part to non-standard programming practice, for example multiple 'data' statements in Fortran subroutines (Steenman-Clark, 2009). Figure 7a shows the difference in mid-Pliocene surface air temperature between our simulation and that of H&V04, and Figure 7b shows the difference in mid-Pliocene surface air temperature *anomaly*, mid-Pliocene minus pre-industrial, between our simulation and that of H&V04. Our mid-Pliocene simulation is significantly cooler than that of H&V04 (-0.8 $^\circ$C in the global annual mean), but the difference in anomalies is smaller (0.3 $^\circ$C). Examination of the temporal evolution of these differences indicates that the effect of hardware and compiler change is more important than the effect of increased spinup time. This underlines the importance of always carrying out sensitivity simulations on the same machine, and with the same compiler, as any control simulation.

As stated in the Introduction, H&V04 estimated the contributions to mid-Pliocene warmth by considering aspects of the global energy balance. Heinemann *et al.* (2009), in the context of the Eocene, present a different method of energy-balance analysis which includes a meridional analysis. Here, we use the method of Heinemann *et al.* (2009) to analyse our mid-Pliocene (E_{ociv}) and pre-industrial (E) simulations. The method gives latitudinal distributions of the contribution to the surface temperature change, $E_{ociv} - E$, of: (a) emissivity changes due to changes in greenhouse gases, (b) emissivity changes due to changes in clouds, (c) albedo changes due to changes in the planetary surface, (d) albedo changes due to changes in clouds, and (e) heat transport changes. This latitudinal partitoning is shown in Figure 5(b). The first thing to note is that this approach is based on zonal and seasonal means, and as such the total surface temperature change is slightly underestimated by the energy balance approach (compare the green line with the black line in Figure 5(b)). On a global scale, the contribution of heat transports to the total change is by definition zero, but in the Northern Hemisphere there is a small positive contribution at high latitudes and a small negative contribution at low latitudes, consistent with a slight increase in poleward heat transport. The global mean contribution of clouds (both albedo and emmissivity effects) is relatively small, but in the short-wave this results from a cancellation of a positive contribution in the tropics and a negative contribution at mid-high latitudes. Changes in emmissivity (due to the increase in greenhouse gas from 280 to 400ppmv, and the associated water vapour forcing) contributes 61% of the total surface temperature change, with greatest contribution in mid-high latitudes. Surface albedo changes contribute 44%, due almost entirely to mid-high latitude changes; in the tropics the change in albedo contributes very little. Overall it can be seen that surface albedo and direct greenhouse-gas forcing are the greatest contributors to the total change, with the greehouse gas forcing dominating in low latitudes, and the surface albedo changes dominating at mid-high latitudes. The polar amplification is significantly dampened by changes in short-wave cloud forcing. It should be noted that cloud processes are amongst the most uncertain in GCMs, and so these results are likely to be model dependent.

5 Discussion

Here we discuss some of the assumptions in this work, including quantitative estimates of how some of these assumptions could affect our results.

5.1 Palaeoenvironmental boundary conditions

In section 3.2 we describe why we use the PRISM2 boundary conditions as opposed to the PRISM3 boundary conditions. The most significant effect of this is likely related to the different orography dataset in PRISM3 compared to PRISM2 (the ice sheets, although different, are similar in extent and height, and the PRISM3 vegetation is based on an extended dataset which includes PRISM2 as a subset). PRISM3 orography is based on the reconstruction of Markwick (2007). It differs from PRISM2 mainly in the high Eurasian latitudes and the Himalayas where the geological evidence is inconclusive and debated (e.g. Rowley and Garzione, 2007; Spicer *et al.*, 2003). The Markwick (2007) reconstruction is actually much closer to modern than that of PRISM2. Therefore, using modern orography instead of PRISM2 provides an end-member approximation for the uncertainty in our results. In this case, given the linearity of the system highlighted in Section 4, the total mid-Pliocene temperature change can be approximated by:

$$\Delta T^{noorog} = \Delta T - dT_{orog} = dT_{CO_2} + dT_{veg} + dT_{ice} \quad (14)$$

which is 2.6 °C. Then, the partitioning (Table 1) is 1.6°C (61%) from the CO_2 (dT_{CO_2}), 0.7°C (27%) is from the vegetation (dT_{veg}), and 0.3°C (13%) from the ice sheets (dT_{ice}).

There is no information given in either PRISM2 or PRISM3 on possible bathymetric differences between the mid-Pliocene and present. As such, we use modern bathymetry in the simulations presented here. However, geophysical records of mantle temperature beneath the North Atlantic indicate that the Greenland-Scotland ridge was about 300 m lower in the Pliocene than modern (Robinson *et al.*, 2011). A recent modelling study (Robinson *et al.*, 2011) has shown that, although this has negligible effect on the global mean temperature, it could lead to increased polar warmth (greater than 5 °C) in the mid-Pliocene due to increased oceanic northward heat transport in the North Atlantic. This has the effect of bringing the modelled SSTs in the mid-Pliocene E_{ociv} simulation into better agreement with the PRISM3 proxy estimates in this region.

5.2 Mid-Pliocene CO_2

Mid-Pliocene atmospheric CO_2 has been reconstructed by a variety of proxies. A value of 400 ppmv has been used in this and several other previous modelling studies of the mid-Pliocene climate (including H&V04), but there are uncertainties in this figure. For example, based on measurements of δ^{13}C in ocean sediments, Raymo *et al.* (1996) cite a mean value of 380 ppmv with maxima as high as 425ppmv. More recent data from Seki *et al.* (2010), using alkenones and boron isotope proxies, cite a mean of 360 ppmv with uncertainties +- 30 ppmv. Other recent data (Pagani *et al.*, 2010) supports a mean of 380 ppmv. As such, for consistency with previous work, and to account for likely associated increases in non-CO_2 greenhouse gases such as are observed in the ice core record (Siegenthaler *et al.*, 2005), we consider here the effects of 350 and 450 ppmv as alternative CO_2 concentrations. To first order, the temperature effects of elevated CO_2 are expected to scale logarithmically with the CO_2 concentration. Therefore, it is possible to estimate the total mid-Pliocene temperature change for an arbitrary CO_2 level of x, $\Delta T^{CO_2=x}$ as:

$$\Delta T^{CO_2=x} = dT_{orog} + dT_{veg} + dT_{ice} + \frac{log(x/280)}{log(400/280)} dT_{co2} \tag{15}$$

For a CO_2 level of 350 ppm this gives $\Delta T^{CO_2=350}$ =2.7 °C, and a partitioning (see Table 1) of 1.0°C (36%) from the CO_2 (dT_{CO_2}), 0.7°C (26%) from the orography, 0.7°C (26%) from the vegetation (dT_{veg}), and 0.3°C (12%) from the ice sheets (dT_{ice}). For a CO_2 level of 450 ppm this gives $\Delta T^{CO_2=350}$ =3.8 °C, and a partitioning (see Table 1) of 2.1°C (55%) from the CO_2 (dT_{CO_2}), 0.7°C (18%) from the orography, 0.7°C (18%), from the vegetation (dT_{veg}), and 0.3°C (9%) from the ice sheets (dT_{ice}).

Furthermore, given a 'true' mid-Pliocene global mean temperature change, $\Delta T^{CO_2=x}$, we can solve Equation 15 for x. By converting the PRISM3 estimates of global SST to estimates of global surface air temperature using a scaling factor, Lunt *et al.* (2010a) estimated the true $\Delta T^{CO_2=x}$ to be about

0.27 °C greater than the ΔT predicted by the model. This allows us to estimate x, the 'true' value of mid-Pliocene CO_2, to be 380 ppmv. It should be noted that this calculation assumes that our uncertainty in CO_2 is much greater than uncertainties which arise due to model error, errors in the applied mid-Pliocene boundary conditions, and errors in the PRISM3 SSTs.

5.3 Climate variability through the mid-Pliocene

The mid-Pliocene spans approximately 300,000 years, and, although relatively stable compared to the Quaternary, does display climate variability on orbital timescales (Lisiecki and Raymo, 2005), which can be interpreted as a series of glacials and interglacials (albeit much smaller in magnitude than those of the Quaternary). By combining high resolution mid-Pliocene oxygen isotope and Mg/Ca measurements, Dwyer and Chandler (2009) identified six sea level highstands during the mid-Pliocene of between 10 and 30 m above modern, and several lowstands, including Marine Isotope Stage KM2 in the middle of the mid-Pliocene, estimated to be 40 m below modern. However, we carry out a single simulation to represent this entire time period.

For the orography, this is probably not an issue, as changes in orography occur over much longer timescales than orbital fluctuations. However, the orbit, CO_2, ice sheets, and vegetation likely varied significantly through the mid-Pliocene. The orbital forcing in our simulations is that of modern. At 65°N in June, the modern forcing is close to the average forcing of the mid-Pliocene, the difference being -15 Wm^{-2} compared to a maximum difference of +50 Wm^{-2} during the mid-Pliocene (Lunt *et al.*, 2008). For CO_2, we have used 400ppmv whereas the record of Raymo *et al.* (1996) varies between 330 and 425 ppmv. For ice sheets, the PRISM2 reconstruction is characterised by a sea-level *increase* of 25m compared to modern, whereas Dwyer and Chandler (2009) find variations in global sea-level of +- 25m compared to modern, encompassing glacial/interglacial variability. The PRISM3 SST evaluation dataset does consist of sub-orbitally dated sites. However, the PRISM SSTs do not represent average SSTs through the mid-Pliocene but have been filtered via a process of 'warm peak averaging' (Dowsett *et al.*, 2009), which means that the PRISM3 SSTs represent average warm interglacial conditions in the mid-Pliocene. For vegetation, the data sites in the Thomson and Fleming reconstruction, upon which PRISM2 are based, are not dated to orbital timescale accuracy, and so each site could represent either glacial or interglacial-type conditions. The same is true of the Salzmann *et al.* (2008) vegetation dataset, with which our simulation has been evaluated. However, in locations where a number of possible biomisations were consistent with the data, Salzmann *et al.* (2008) chose the warmest, to maintain consistency with the SST warm peak averaging.

As such, our simulations are a hybrid representation of the mid-Pliocene: the orbit, vegetation and orography being close to mid-Pliocene average, and the CO_2 and ice sheets being closer to interglacial values. The mid-Pliocene simulation has previously been compared with vegetation data which represent an average-to-warm mid-Pliocene palaeoenvironment (Lunt *et al.*, 2010a), and SST data which represent interglacial values (Dowsett *et al.*, 2011). These discrepancies may go some way to explaing some of the model-data disagreements. For example, the greater high-latitude warmth in the PRISM SST reconstruction compared to the model could be a result of the warm-peak averaging, which by definition biases the SST reconstructions to warm values. Future work will aim to carry out simulations more representative of specific time periods within the mid-Pliocene, and to compare these to orbitally-resolved versions of the PRISM SST dataset.

5.4 Model uncertainties

Uncertainties associated with the model itself (as opposed to the boundary condition uncertainties discussed above) can be broadly divided into 'parametric uncertainty' and 'structural uncertainty'.

Parametric uncertainty relates to uncertainties in model parameters. These parameters are often associated with the representation of sub-gridscale processes and include, for example, the gridbox-average relative humidity at which clouds are assumed to start forming. They are generally poorly constrained by observations and so are essentially ‘tunable’. A single model simulation, as presented in this paper, can only represent one single point in the whole space of possible plausible parameter combinations, and as such undersamples the range of model possibilities. The full space can be explored by carrying out simulations in which these tunable parameters are perturbed. A preliminary study has been carried out with this model in the context of the mid-Pliocene (Pope *et al.*, 2011). That study found a range of ΔT of 2.7 °C to 4.5 °C and could therefore be used to place approximate error bars on our ΔT; however, it did not investigate the causes of such a change, so the impact of uncertain parameters on our factorisation is unclear, and is a focus of ongoing work.

Structural uncertainty relates to changes in the model which can not be made purely by modifying the values of tunable parameters. It relates to our uncertainty in the physical processes themselves which govern Earth System behavior, and our inability to implement complex processes in a numerical model of a given resolution. Some information on the magnitude of this error can be obtained by considering other climate models. Haywood *et al.* (2009) compared two structurally different models, of the mid-Pliocene. They had a range of ΔT of 2.39°C to 2.41 °C (this is very much a minimum uncertainty range, especially as those simulations were carried out with atmosphere-only models). Again, while putting some context to our results, it is not clear how this uncertainty would affect our factorisation or energy balance analysis. Ongoing work, in the framework of the project PlioMIP, is aiming to gain more information on the structural uncertainty by comparing many atmosphere-only and atmosphere-ocean Pliocene simulations produced by different models (Haywood *et al.*, 2010, 2011b).

6 Conclusions

Using a novel form of factorisation, we have partitioned the causes of mid-Pliocene warmth between CO_2 (36% - 61%), orography (0-26%), vegetation (21%-27%) and ice sheets (9-13%). The ranges are estimated by considering the sensitivity of the results to uncertainties in the mid-Pliocene CO_2 concentration and orography (summarised in Table 1). Despite the relatively small contribution of ice sheets on a global scale, it is responsible for the majority of Southern Hemisphere high latitude warming. Northern Hemisphere high-latitude warming is due mainly to a combination of CO_2 and orography changes. Furthermore, we have carried out an energy balance analysis, and shown that surface albedo changes and direct greenhouse-gas forcing contribute significantly more than cloud feedbacks to the total mid-Pliocene warming, with the greehouse gas forcing dominating in low latitudes, and the surface albedo changes dominating at mid-high latitudes.

Future work should further assess the sensitivity of these results to the boundary conditions applied (for example by using the newer PRISM3 reconstructions compared with PRISM2 used here, and extending the datasets to include varying soil properties), to the model used, and to parameters within the models themselves. Both the modelling and data communities should start to investigate orbital-scale variability within the mid-Pliocene. This is particularly important for assessing the real relevance of the mid-Pliocene as an analogue for long-term future (sub-orbital timescale) climate change.

References

Bonham, S. G., Haywood, A. M., Lunt, D. J., Collins, M., and Salzmann, U. (2009). El Nino-Southern Oscillation, Pliocene climate and equifinality. *Phil. Trans. R. Soc. A,*, **367**, 127–156.

Braconnot, P., Otto-Bliesner, B., Harrison, S., Joussaume, S., Peterchmitt, J.-Y., Abe-Ouchi, A., Crucifix, M., Driesschaert, E., Fichefet, T., Hewitt, C. D., Kageyama, M., Kitoh, A., Lan, A., Loutre, M.-F., Marti, O., Merkel, U., Ramstein, G., Valdes, P., Weber, S. L., Yu, Y., and Zhao, Y. (2007). Results of pmip2 coupled simulations of the mid-holocene and last glacial maximum ? part 1: experiments and large-scale features. *Clim. Past*, **3**, 261–277.

Broccoli, A. J. and Manabe, S. (1987). The influence of continental ice, atmospheric co2, and land albedo on the climate of the last glacial maximum. *Clim. Dyn.*, **1**, 87–99.

Cattle, H. and Crossley, J. (1995). Modelling Arctic climate change. *Philosophical Transactions of the Royal Society of London A*, **352**, 201–213.

Cohen, J. (1960). A coefficient of agreement for nominal scales. *Educational and Psychological Measurement*, **2**, 37–46.

Cox, P., Betts, R., Bunton, C., Essery, R., Rowntree, P. R., and Smith, J. (1999). The impact of new land-surface physics on the GCM simulation and climate sensitivity. *Climate Dynamics*, **15**, 183–203.

Cronin, T. M., Whatley, R. C., Wood, A., Tsukagoshi, A., Ikeya, N., Brouwers, E. M., and Briggs, W. M. (1993). Microfaunal evidence for elevated mid-Pliocene temperatures in the arctic ocean. *Paleoceanography*, **8**, 161–173.

Dolan, A. M., Haywood, A. M., Hill, D. J., Dowsett, H. J., Lunt, D. J., and Pickering, S. J. (2011). Sensitivity of pliocene ice sheets to orbital forcing. *Palaeogeography, Palaeoclimatology, Palaeoecology*, **309**, 98–110.

Dowsett, H. and Willard, D. A. (1996). Southeast Atlantic marine and terrestrial response to middle Pliocene change. *Mar. Micropaleontol.*, **27**, 181–193.

Dowsett, H. J. (2007). The PRISM palaeoclimate reconstruction and Pliocene sea-surface temperature. In M. Williams, A. M. Haywood, J. F. Gregory, and D. N. Schmidt, editors, *Deep time perspectives on climate change: marrying the signal from computer models and biological proxies*, pages 459–480. The Micropalaeontological Society Special Publications, Geological Society of London.

Dowsett, H. J. and Cronin, T. M. (1990). High eustatic sea level during the middle Pliocene: Evidence from the southeastern u.s. atlantic coastal plain. *Geology*, **18**, 435–438.

Dowsett, H. J. and Poore, J. A. B. H. R. (1996). Middle pliocene sea surface temperatures: a global reconstruction. *Marine Micropaleontology*, **27**, 13–25.

Dowsett, H. J., Cronin, T. M., Poore, P. Z., Thompson, R. S., Whatley, R. C., and Wood, A. M. (1992). Micropaleontological evidence for increased meridional heat-transport in the north atlantic ocean during the pliocene. *Science*, **258**, 1133–1135.

Dowsett, H. J., Thompson, R. S., Barron, J. A., Cronin, T. M., Fleming, R. F., Ishman, S. E., Poore, R. Z., Willard, D. A., and Holtz, T. R. (1994). Joint investigations of the middle Pliocene climate I: PRISM paleoenvironmental reconstructions. *Global and Planetary Change*, **9**, 169–195.

Dowsett, H. J., Barron, J. A., Poore, R. Z., Thompson, R. S., Cronin, T. M., Ishman, S. E., and Willard, D. A. (1999). Middle Pliocene paleoenvironmental reconstruction: PRISM2. *USGS Open File Report 99-535*, pages http://pubs.usgs.gov/of/1999/of99–535/.

Dowsett, H. J., Robinson, M. M., and Foley, K. M. (2009). Pliocene three-dimensional global ocean temperature reconstruction. *Climate of the Past*, **5**, 769–783.

Dowsett, H. J., Robinson, M. M., Stoll, D. K., and Foley, K. M. (2010a). Mid-Piacenzian mean annual sea surface temperature analysis for data-model comparisons. *Stratigraphy*, **7**, 189–198.

Dowsett, H. J., Robinson, M. M., Haywood, A. M., Salzmann, U., Hill, D., Sohl, L., Chandler, M., Williams, M., Foley, K., and Stoll, D. K. (2010b). The prism3d paleoenvironmental reconstruction. *Stratigraphy*, **7**, 123–139.

Dowsett, H. J., Haywood, A. M., Valdes, P. J., Robinson, M. M., Lunt, D. J., Hill, D., Stoll, D. K., and Foley, K. (2011). Sea surface temperatures of the mid-piacenzian warm period: A comparison of prism3 and hadcm3. *Palaeogeography, Palaeoclimatology, Palaeoecology*, **309**, 83–91.

Dwyer, G. S. and Chandler, M. A. (2009). Mid-pliocene sea level and continental ice volume based on coupled benthic mg/ca palaeotemperatures and oxygen isotopes. *Phil. Trans. R. Soc. A*, **367**, 157–168.

Edwards, J. M. and Slingo, A. (1996). Studies with a flexible new radiation code 1: Choosing a configuration for a large-scale model. *Quaterly Journal of the Royal Meteorological Society*, **122**, 689–719.

Fedorov, A. V., Brierley, C. M., and Emanuel, K. (2010). Tropical cyclones and permanent el nio in the early pliocene epoch. *Nature*, **463**, 1066–1070.

Fleming, R. F. and Barron, J. A. (1996). Evidence of Pliocene Notofagus in Antarctica from Pliocene marine sedimentary deposits (DSDP Site 274). *Mar. Micropaleontol.*, **27**, 227–236.

Foster, G. L., Lunt, D. J., and Parrish, R. R. (2010). Mountain uplift and the glaciation of north america - a sensitivity study. *Clim. Past*, **6**, 707–717.

Gent, P. R. and McWilliams, J. C. (1990). Isopycnal mixing in ocean circulation models. *Journal of Physical Oceanography*, **20**(1), 150–155.

Gordon, C., Cooper, C., Senior, C. A., Banks, H., Gregory, J. M., Johns, T. C., Mitchell, J. F. B., and Wood, R. A. (2000). The simulation of SST, sea ice extents and ocean heat transports in a version of the Hadley Centre coupled model without flux adjustments. *Climate Dynamics*, **16**(2-3), 147–168.

Gregory, D., Kershaw, R., and Inness, P. M. (1997). Parametrisation of momentum transport by convection II: tests in single column and general circulation models. *Quarterly Journal of the Royal Meteorological Societ*, **123**, 1153–1183.

Gregory, J. M. and Mitchell, J. F. B. (1997). The climate response to CO_2 of the hadley centre coupled aogcm with and without flux adjustment. *Geophysical Research Letters*, **24**, 1943–1946.

Harrison, S. P. and Prentice, I. C. (2003). Climate and co_2 controls on global vegetation distribution at the last glacial maximum: analysis based on palaeovegetation data, biome modelling and palaeoclimate simulations. *Global Change Biology*, **9**, 983–1004.

Haxeltine, A. and Prentice, I. C. (1996). BIOME3: an equilibrium terrestrial biosphere model based on ecophysiological constrains, resource availability, and competition among plant functional types. *Global Biogeochemical Cycles*, **10**, 693–709.

Haywood, A. M. and Valdes, P. J. (2004). Modelling Middle Pliocene warmth: Contribution of atmosphere, oceans and cryosphere. *Earth and Planetary Science Letters*, **218**, 363–377.

Haywood, A. M., Valdes, P. J., and Sellwood, B. W. (2000a). Global scale palaeoclimate reconstruction of the middle pliocene climate using the ukmo gcm: initial results. *Global and Planetary Change*, **28**, 239–256.

Haywood, A. M., Sellwood, B. W., and Valdes, P. J. (2000b). Regional warming: Pliocene (3 ma) paleoclimate of europe and the mediterranean. *Geology*, **28**, 1063–1066.

Haywood, A. M., Chandler, M. A., Valdes, P. J., Salzmann, U., Lunt, D. J., and Dowsett, H. J. (2009). Comparison of mid-pliocene climate predictions produced by the hadam3 and gcmam3 general circulation models. *Global and Planetary Change*, **66**, 208–224.

Haywood, A. M., Dowsett, H. J., Otto-Bliesner, B., Chandler, M. A., Dolan, A. M., Hill, D. J., Lunt, D. J., Robinson, M. M., Rosenbloom, N., Salzmann, U., and Sohl, L. E. (2010). Pliocene Model Intercomparison Project (PlioMIP): experimental design and boundary conditions (Experiment 1). *Geoscientific Model Development*, **3**, 227–242.

Haywood, A. M., Ridgwell, A., Lunt, D. J., Hill, D. J., Pound, M. J., Dowsett, H. J., Dolan, A. M., Francis, J. E., and Williams, M. (2011a). Are there pre-quaternary geological analogues for a future greenhouse warming? *Phil. Trans. R. Soc. A*, **369**, 933–956.

Haywood, A. M., Dowsett, H. J., Robinson, M. M., Stoll, D. K., Dolan, A. M., Lunt, D. J., Otto-Bliesner, B., and Chandler, M. A. (2011b). Pliocene Model Intercomparison Project (PlioMIP): experimental design and boundary conditions (Experiment 2). *Geoscientific Model Development*, **4**, 571–577.

Heinemann, M., Jungclaus, J. H., and Marotzke, J. (2009). Warm Paleocene/Eocene climate as simulated in ECHAM5/MIO-OM. *Climate of the Past*, **5**, 785–802.

Hibler, W. D. (1979). A dynamic thermodynamic sea ice model. *Journal of Physical Oceanography*, **9**, 815–846.

Hill, D. J., Haywood, A. M., Hindmarsh, R. C. A., and Valdes, P. J. (2007). *Deep time perspectives on climate change: marrying the signal from computer models and biological proxies*, chapter Characterising ice sheets during the mid Pliocene: evidence from data and models. The Micropalaeontological Society Special Publications, Geological Society of London.

Hill, D. J., Dolan, A. M., Haywood, A. M., Hunter, S. J., and Stoll, D. K. (2010). Sensitivity of the greenland ice sheet to pliocene sea surface temperatures. *Stratigraphy*, **7**, 111–122.

Huybrechts, P., Gregory, J. M., Janssens, I., and Wild, M. (2004). Modelling antarctic and greenland volume changes during the 20th and 21st centuries forced by gcm time slice integrations. *Global and Planetary Change*, **42**, 83–105.

Jahn, A., Claussen, M., Ganopolski, A., and Brovkin, V. (2005). Quantifying the effect of vegetation dynamics on the climate of the last glacial maximum. *Clim. Past*, **1**, 1–7.

Jansen, E., Overpeck, J., Briffa, K. R., Duplessy, J. C., Joos, F., Masson-Delmotte, V., Olago, D., Otto-Bliesner, B., Peltier, W. R., Rahmstorf, S., Ramesh, R., Raynaud, D., Rind, D., Solomina, O., Villalba, R., and Zhang, D. (2007). *Climate Change 2007: The Physical Science Basis. Contribution of Working Group I to the Fourth Assessment Report of the Intergovernmental Panel on Climate Change*, chapter Paleoclimate. Cambridge University Press.

Kaplan, J. O. (2001). *Geophysical applications of vegetation modeling*. Ph.D. thesis.

Kohfeld, K. E. and Harrison, S. P. (2000). How well can we simulate past climates? Evaluating the models using global palaeoenvironmental datasets. *Quaternary Science Reviews*, **19**, 321–346.

Kutzbach, J. E., Guetter, P. J., Ruddiman, W. F., and Prell, W. L. (1989). Sensitivity of climate to Late Cenozoic uplift in southern Asia and the American West: Numerical experiments. *Journal of Geophysical Research (Atmos.)*, **94**, 18393–18407.

Lisiecki, L. E. and Raymo, M. E. (2005). A Pliocene-Pleistocene stack of 57 globally distributed benthic δ^{18}O records. *Paleoceanography*, **20**, doi:10.1029/2004PA001071.

Lunt, D. J., de Noblet-Ducoudre, N., and Charbit, S. (2004). Effects of a melted greenland ice sheet on climate, vegetation, and the crysophere. *Climate Dynamics*, **23**, 679–694.

Lunt, D. J., Foster, G. L., Haywood, A. M., and Stone, E. J. (2008). Late Pliocene Greenland glaciation controlled by a decline in atmospheric CO_2 levels. *Nature*, **454**, 1102–1105.

Lunt, D. J., Haywood, A. M., Schmidt, G. A., Salzmann, U., Valdes, P. J., and Dowsett, H. J. (2010a). Earth system sensitivity inferred from Pliocene modelling and data. *Nature Geoscience*, **3**, 60–64.

Lunt, D. J., Flecker, R., and Clift, P. D. (2010b). The impacts of Tibetan uplift on palaeoclimate proxies. *Geological Society, London, Special Publications*, **342**, 279-291.

Markwick, P. J. (2007). *Deep time perspectives on climate change: marrying the signal from computer models and biological proxies*, chapter The palaeogeographic and palaeoclimatic significance of climate proxies for data-model comparisons. The Micropalaeontological Society Special Publications, Geological Society of London.

Matthews, E. (1985). Prescription of land-surface boundary conditions in GISS GCM II: a simple method based on high-resolution vegetation data bases. *NASA Report*, **TM 86096**, 20.

Monserud, R. A. and Leemans, R. (1992). Comparing global vegetation maps with the kappa statistic. *Ecological Modelling*, **62**, 275–293.

Naish, T. R. and Wilson, G. S. (2009). Constraints on the amplitude of Mid-Pliocene (3.6-2.4 Ma) eustatic sea-level fluctuations from the New Zealand shallow-marine sediment record. *Phil. Trans. R. Soc. A*, **367**, 169–187.

Pagani, M., Liu, Z., LaRiviere, L., and Ravelo, A. C. (2010). High Earth-system climate sensitivity determined from Pliocene carbon dioxide concentrations. *Nature Geoscience*, **3**, 27–30.

Pollard, D. and DeConto, R. M. (2009). Modelling west antarctic ice sheet growth and collapse through the past five million years. *Nature*, **458**, 329–332.

Pope, J. O., Collins, M., Haywood, A., Dowsett, H., Hunter, S., Lunt, D., Pickering, S., and Pound, M. (2011). Quantifying uncertainty in model predictions for the pliocene (plio-qump): Initial results. *Palaeogeography, Palaeoclimatology, Palaeoecology*, **309**, 128–140.

Raymo, M. E., Grant, B., Horowitz, M., and Rau, G. H. (1996). Mid-Pliocene warmth: stronger greenhouse and stronger conveyor. *Marine Micropaleontology*, **27**, 313–326.

Robinson, M. (2009). New quantitative evidence of extreme warmth in the Pliocene Arctic. *Stratigraphy*, **6**, 265–275.

Robinson, M., Valdes, P. J., Haywood, A. M., Dowsett, H. J., Hill, D. J., and Jones, S. M. (2011). Bathymetric controls on Pliocene North Atlantic and Arctic sea surface temperature and deepwater production. *Palaeogeography, Palaeoclimatology, Palaeoecology*, **309**, 92–97.

Rowley, D. B. and Garzione, C. N. (2007). Stable isotope-based paleoaltimetry. *Annual Review of Earth and Planetary Sciences*, **35**, 463–508.

Salzmann, U., Haywood, A. M., Lunt, D. J., Valdes, P. J., and Hill, D. J. (2008). A new global biome reconstruction for the Middle Pliocene. *Global Ecology and Biogeography*, **17**, 432–447.

Salzmann, U., Haywood, A. M., and Lunt, D. J. (2009). The past is a guide to the future? Comparing Middle Pliocene vegetation with predicted biome distributions for the twenty-first century. *Phil. Trans. R. Soc. A*, **367**, 189–204.

Scroxton, N., Bonham, S. G., Rickaby, R. E. M., Lawrence, S. H. F., Hermoso, M., and Haywood, A. M. (2011). Persistent el nio-southern oscillation variation during the pliocene epoch. *Paleoceanography*, **26**, PA2215.

Seki, O., Foster, G. L., Schmidt, D. N., Mackenden, A., Kawamura, K., and Pancost, R. D. (2010). Alkenone and boron-based Pliocene pCO_2 records. *Earth and Planetary Science Letters*, **292**, 201–211.

Siegenthaler, U., Stocker, T. F., Monnin, E., Luthi, D., Schwander, J., Stauffer, B., Raynaud, D., Barnola, J.-M., Fischer, H., Masson-Delmotte, V., and Jouzel, J. (2005). Stable carbon cycle-climate relationship during the Late Pleistocene. *Science*, **310**, 1313–1317.

Solomon, S., Qin, D., Manning, M., Chen, Z., Marquis, M., and Averyt, K. B. (2007). *Climate Change 2007: The Physical Science Basis. Contribution of Working Group I to the Fourth Assessment Report of the Intergovernmental Panel on Climate Change*. Cambridge University Press.

Spicer, R. A., Harris, N. B. W., Widdowson, M., Herman, A. B., Guo, S., Valdes, P. J., and Wolfe, J. A. (2003). Constant elevation of southern tibet over the past 15 million years. *Nature*, **421**, 622–624.

Steenman-Clark, L. (2009). Compiler Sensitivity Study. *Unpublished*, poster presented at NCAS meeting 2009. Available from http://cms.ncas.ac.uk/index.php/component/docman/doc_download/308-compiler-sensitivity-poster.

Stein, U. and Alpert, P. (1993). Factor separation in numerical simulations. *J. Atmos. Sci.*, **50**, 2107–2115.

Thompson, R. S. and Fleming, R. F. (1996). Middle Pliocene vegetation: reconstructions, paleoclimatic inferences, and boundary conditions for climatic modeling. *Marine Micropaleontology*, **27**, 13–26.

Toniazzo, T., Gregory, J. M., and Huybrechts, P. (2004). Climatic impact of a greenland deglaciation and its possible irreversibility. *Journal of Climate*, **17**, 21–33.

Van Campo, E. V. (1991). Pollen transport into arabian sea sediments. In W. L. Prell and N. Niitsuma, editors, *Proceedings of the Ocean Drilling Program, Scientific Results*, pages 277–281. Ocean Drilling Program, Texas A&M University.

von Deimling, T. S., Ganopolski, A., and Held, H. (2006). How cold was the last glacial maximum? *Geophys. Res. Lett.*, **33**, L14 709.

Watanabe, T., Suzuki, A., Minobe, S., Kawashima, T., Kameo, K., Minoshima, K., Aguilar, Y. M., Wani, R., Kawahata, H., Sowa, K., Nagai, T., and Kase, T. (2011). Permanent el nio during the pliocene warm period not supported by coral evidence. *Nature*, **471**, 209–211.

Willard, D. A. (1994). Palynological record from the North Atlantic region at 3 Ma: vegetational distribution during a period of global warmth. *Review of Paleobotany and Palynology*, **83**, 275–297.

Willard, D. A., Cronin, T. M., Ishman, S. E., and Litwin, R. J. (1993). Terrestrial and marine records of climate and environmental change during the Pliocene in subtropical Florida. *Geology*, **21**, 679–682.

Wohlfahrt, J., Harrison, S. P., and Braconnot, P. (2004). Synergistic feedbacks between ocean and vegetation on mid- and high-latitude climates during the mid-holocene. *Climate Dynamics*, **22**, 223–238.

Acknowledgments DJL is funded by an RCUK fellowship. AMH acknowledges the Leverhulme Trust for the award of a Philip Leverhulme Prize. US received funding from the Natural Environment Research Council (NE/I016287/1). DJL and AMH received funding from the Natural Environment Research Council (NE/G009112/1).

Tables

	ΔT [°C]	dT_{CO_2} [°C]	dT_{orog} [°C]	dT_{ice} [°C]	dT_{veg} [°C]
Default	3.30	1.58	0.70	0.70	0.33
orography = modern	2.60	1.58	0	0.70	0.33
CO_2 = 350ppmv	2.71	0.99	0.70	0.70	0.33
CO_2 = 450ppmv	3.83	2.10	0.70	0.70	0.33

Table 1: Total mid-Pliocene global mean warming compared to preindustrial (ΔT), and the global mean partitioning between CO_2 (dT_{CO_2}), orography (dT_{orog}), vegetation (dT_{veg}), and ice (dT_{ice}). This is shown for the default case, and cases where the sensitivity to orography and CO_2 are tested, as described in Sections 5.1 and 5.2.

Figure Captions

Figure 1: Factor separation for a function of two variables - in this case CO_2 and orography. (a) is the linear approach (Equation 2), (b) is the Stein and Alpert (1993) approach (Equation 5), and (c) is our approach (Equation 7 or Equation 8).

Figure 2: Factor separation used in our study for two functions of two variables each - in this case CO_2, orography, vegetation, and ice (Equation 13).

Figure 3: Orography and snow-free albedo for the E, E_{oci}, E_{ocv}, and E_{ociv} GCM simulations. For equivalent figures of the other GCM simulations (E_o, E_c, and E_{oc}), see Table 1 of Supplementary Information of Lunt *et al.* (2010a).

Figure 4: (a) Simulated annual mean surface air temperature change, mid-Pliocene minus pre-industrial, ΔT. (b-e) Surface air temperature changes due to (b) CO_2 (dT_{CO_2}), (c) orography (dT_{orog}), (d) vegetation (dT_{veg}), and (e) ice (dT_{ice}); as calculated from Equation 13.

Figure 5: Zonal annual mean surface air temperature changes due to CO_2 (dT_{CO_2}), orography (dT_{orog}), vegetation (dT_{veg}), and ice (dT_{ice}) [$^{\circ}$C].

Figure 6: Surface air temperature change due to CO_2 alone calculated as (a) Equation 2 and (b) Equation 3. The difference between the two approaches (equal to the synergy, S in Equation 5) is shown in (c).

Figure 7: (a) Difference in mid-Pliocene surface air temperature between our simulation and that of Haywood and Valdes (2004). (b) The same, but for the mid-Pliocene *anomalies*, mid-Plioene minus pre-industrial.

*Highlights

- First quantification of the relative influences on mid-Pliocene warmth and polar amplification of CO2, orography, vegetation, and ice sheets.
- A new factorisation technique, an improvement on the traditional Stein+Alpert approach.
- A quantitative assessment of the uncertainties in our results.

Figure 1
Click here to download Figure: plio_causes_epsl_3.0_Fig1.pdf

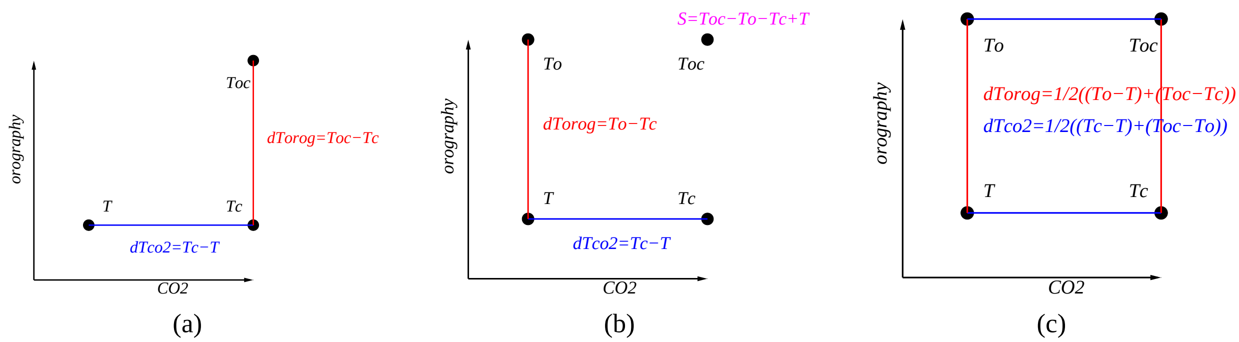

Figure 2
Click here to download Figure: plio_causes_epsl_3.0_Fig2.pdf

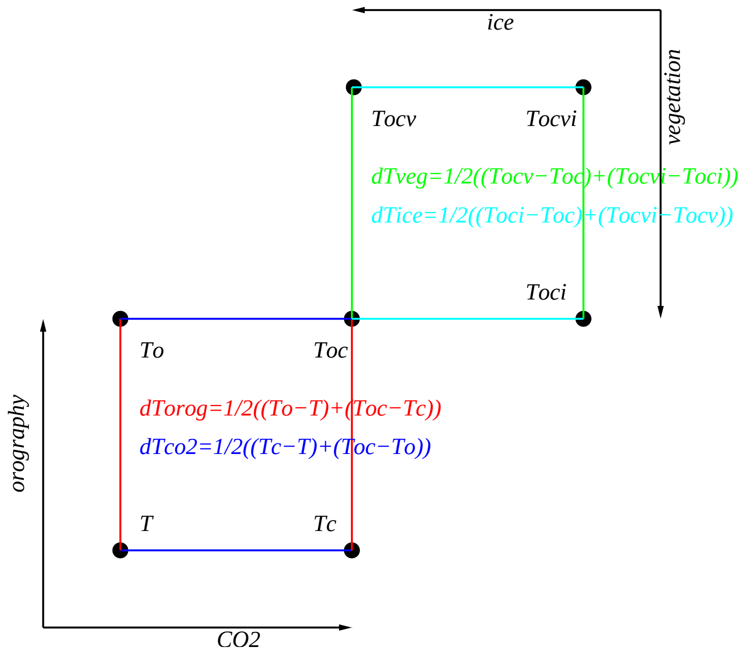

Figure 3

Click here to download Figure: plio_causes_epsl_3.0_Fig3.pdf

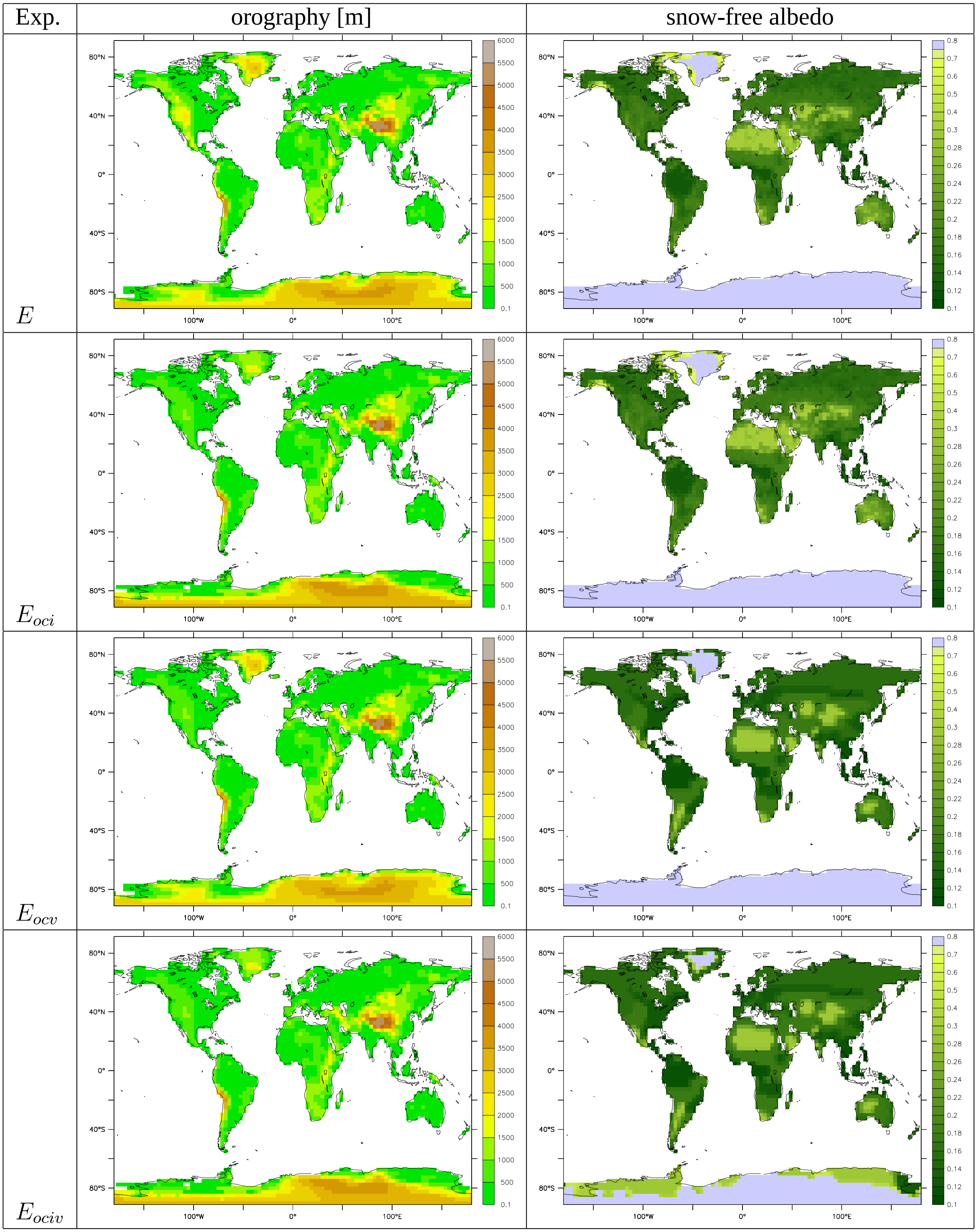

Figure 4

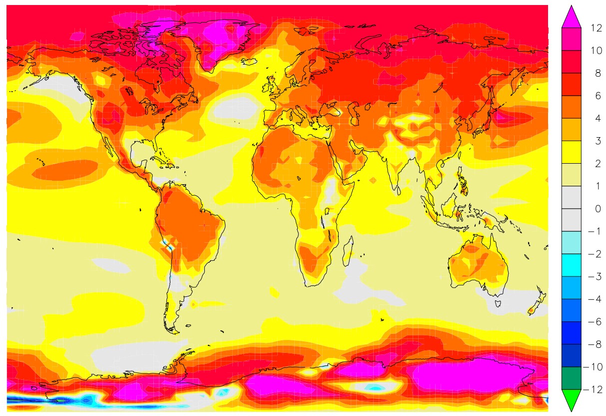

(a)

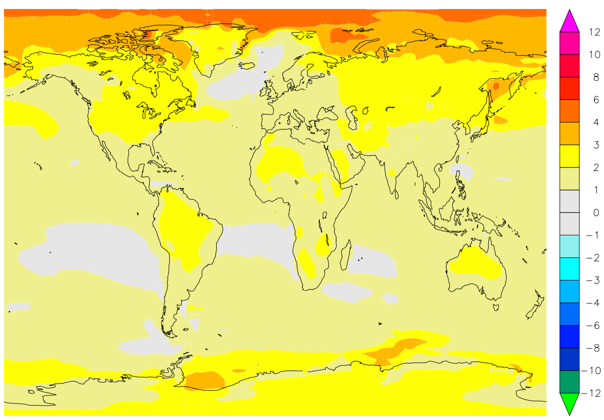

(b)

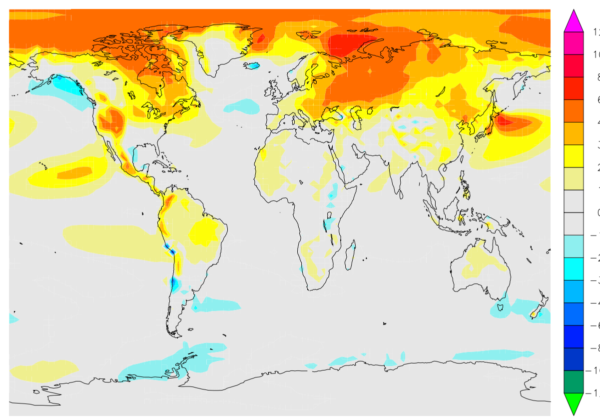

(c)

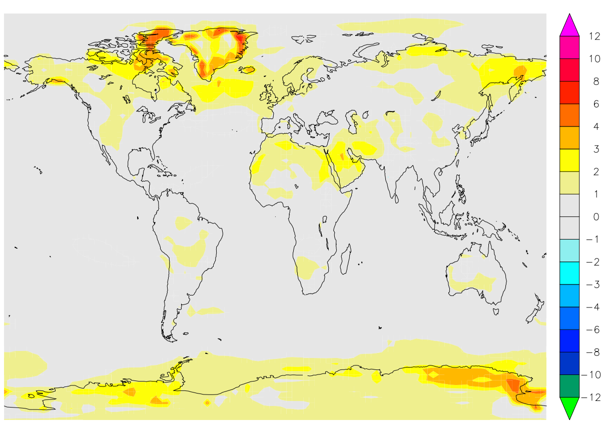

(d)

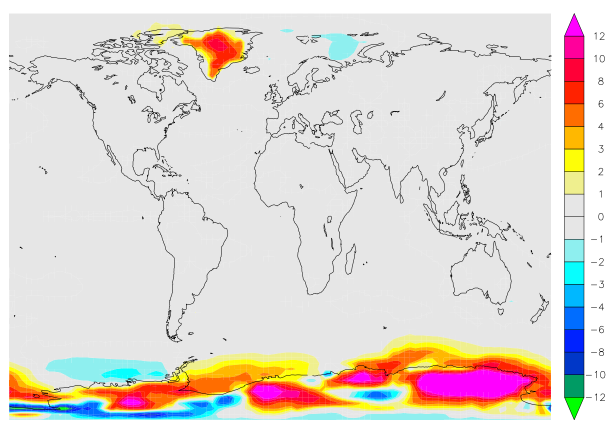

(e)

Figure 5

Click here to download Figure: plio_causes_epsl_3.0_Fig5.pdf

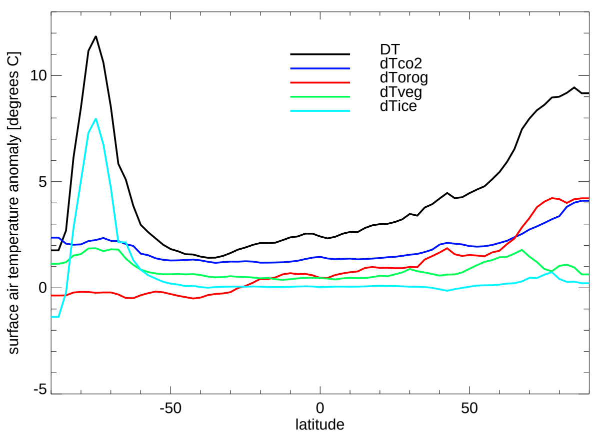

(a)

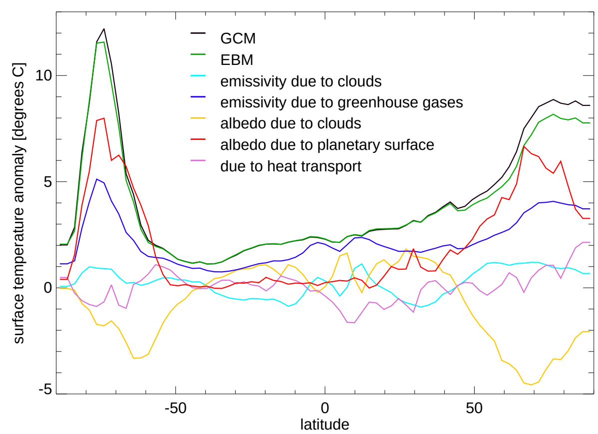

(b)

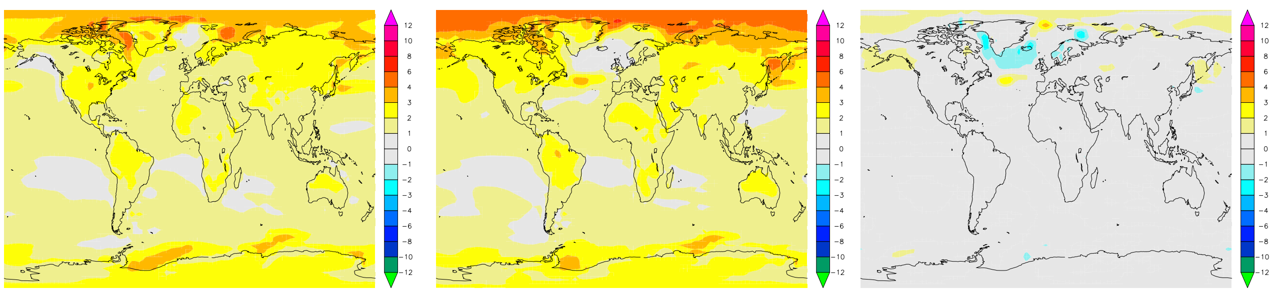

(a) (b) (c)

Figure 7

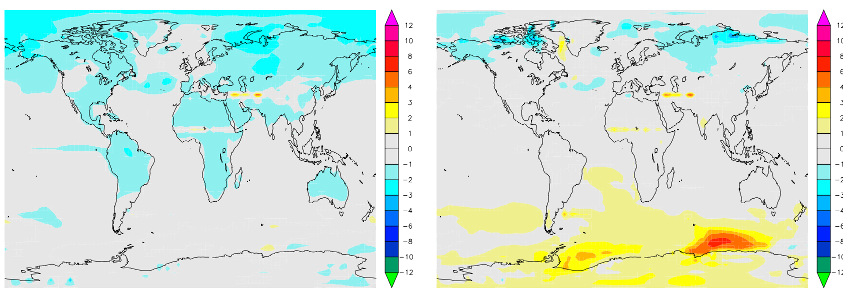

(a) (b)